

Automated Inspection for Remote Telerobotic Operations

K. Venkatesh Prasad

Beckman Laboratories
Division of Biology
California Institute of Technology, 216-76
Pasadena, California 91125

J. Balaram

Robotic Systems and
Advanced Computer Technology Section
Jet Propulsion Laboratory, JW-219
Pasadena, California 91109

Abstract

This paper reports on automated inspection techniques being researched and developed for surface inspection of remote space platforms. The unique problems of performing visual telerobotic inspection in space are identified. An image differencing method to detect changes to surfaces over a period of time is presented together with a scale-space technique for flaw identification. Examples from images of laboratory mockup of space platform modules are presented to illustrate the results.

1 Introduction

The goal is to develop algorithms and software to enable the automated inspection of large space structure surfaces for damage and degradation. The objective is to process sensor data and detect critical anomalies by identifying areas in the image that have changed and to then identify the flaw responsible for the change. The flaws to be inspected include damage from micro meteorites and space debris; material degradation due to exposure to mono atomic oxygen, solar wind, UV radiation, and thermal cycling effects; geometrical mismatches at mechanical interfaces; fluid (hydrazine) leaks; and thermal anomalies. Detection is to be performed under harsh and changing orbital lighting conditions, with highly specular materials and at a safe collision-free operational distance. The objective is to augment a human operator's inspection activities and not necessarily to replace them. An automated system would in effect perform like a "mine detector" that could be scanned across the surface of the object, with the final determination of the flaw being made by the operator.

The aim is to facilitate periodic remote inspection

and monitoring of space structures such as the Space Station Freedom (SSF), using minimal crew Extra Vehicular Activity (EVA) and instead relying on on-board supervised robotic capability. The SSF is a large space platform with complex mechanical, electrical, thermal, fluid and gas interfaces, and changing suite of internal and external scientific experimental apparatus. Over a 30 year design lifetime, on-orbit maintenance of such a complex, changing facility requires periodic as well as "on demand" inspection capabilities. Although subjective "eyes-on" observations during planned crew-EVA will gather much important data, telerobotic inspection offers precise repetition of calibrated sensor placement and positioning, enhanced (non-visible light) sensing, digital scene recording and matching, and greater automation in flaw detection and categorization. Cost savings from reduction in EVA times, relief from boredom and fatigue are also enabled by automated inspection and monitoring tools. Although the ground-based control of robotic devices is not currently part of the SSF baseline design, the National Aeronautics and Space Administration (NASA) is interested in performing a feasibility study to determine if future ground-based telerobotic operations can supplement on-board operations.

1.1 Inspection Problems

Much of the existing data on the effects of the space environment has been obtained from the Long Duration Exposure Facility (LDEF) flown by NASA. The LDEF spacecraft was a 10 meter long, 6 meter diameter, 14-faced open-grid structure on which a series of 86 rectangular trays were used to mount experiment hardware. The spacecraft was exposed to the on-orbit space environment for 6 years at low earth orbit. Preliminary data from the LDEF spacecraft [1] analyzes more

than 34,000 impact features ranging in size from 5.7 millimeter diameter to 0.1 micrometers. This data has allowed the determination of how surface orientation alters the rate of surface impact, flux rates for man-made and natural impacts, rate of increase of space debris, and the morphological features of the surface flaws as a function of the impactor and impacted materials.

Although at the present time, detailed SSF inspection requirements have not been specified (except for SSF utility tray cables), NASA has emphasized the need for inspection in various documents and forums. For example, the SSF External Maintenance Task Team Final Report [2], Appendix E, specifies high-level requirements for the inspection of the station and states that telerobotics should be utilized to accomplish some of the inspection tasks. A number of candidate tasks have been identified based on our interactions with engineers at the Johnson Space Center and various scientists working with data from the Long Duration Exposure Facility (LDEF). These include inspection of: (1) truss strut damaged by micro meteoroids (2) cracks in structures (3) shield area damaged by micro meteoroids (4) thermal blankets, radiators, or solar panels damaged by micro meteoroids and atomic oxygen (5) thermal/mechanical interfaces at Orbital Replacement Unit (ORU) installation sites (6) deployable mechanisms for incorrectly positioned latches, connectors, and other mechanical devices (7) the SSF shuttle docking port before each docking (8) damaged fluid and power lines in utility trays (9) effects of fluid leaks on optics (10) magnetic field, plasma fields, and contaminant levels, especially hydrazine concentration. For telerobotic surface inspection of flaws, detection of impact features in the range of 0.2 to 6.0 mm appears to be adequate for safety monitoring the SSF.

At the Jet Propulsion Laboratory (JPL), NASA has established a Remote Surface Inspection Laboratory to develop and demonstrate technology for telerobotic inspection. The laboratory integrates manipulation, sensing and operator interface technology in a single inspection system and provides a simulated spacecraft and orbital lighting mockup for the performance of inspection experiments, both automated and human tele-operated. A near real-time system for flaw detection using a I image differencing approach is currently operational at JPL and allows the monitoring of changes to ORU modules. The inspection system allows the operator supervised scanning of an ORU surface, the detection of various flaws, and an archival/cataloging system to track and monitor flaw progression. Various technologies in 7-dof arm control, base/robot mobil-

ity coordination, collision detection and avoidance, are part of this effort and are described in [3, 4]. However, the emphasis in this paper is on the automated inspection components of the system. The technology and hardware/software developed at JPL is then to be transferred to the NASA Johnson Space Center (JSC) for subsequent integration into the JSC Space Station robotics facilities. Two other inspection programs are currently underway at NASA at the Kennedy Space Center. These are the *Shuttle Radiator Assembly Inspection* and *Shuttle Tile Inspection* tasks. These inspection efforts are however terrestrial applications and do not have to contend with some of the unique features of performing inspection operations in space.

2.1 Inspection Technical Issues

Automated visual inspection is widely used in industrial manufacturing for product inspection for functional and cosmetic effects [5, 6]. A number of technical and operational issues provide unique technical challenges to telerobotic inspection of space platforms. We briefly describe these issues and describe how they impact the imaging hardware and experimental setup.

1. Solar illumination at near earth orbit is approximately 131,000 lux. The absence of atmospheric dispersion results in shadowed regions that tend to be very dark. In the laboratory, simulated solar illumination at approximately 10 percent of the true solar intensity is used in the interests of minimizing the safety risks associated with high power lights. As a consequence, the controlled illumination that is utilized in the laboratory must also be similarly scaled down. The ambient light is provided using a 1200W, 5600:1400K, adjustable-focus Luxarc 1200 lamp and produces high contrast between shadowed and lit surfaces.
2. Solar illumination at low earth orbit varies as the spacecraft traverses its orbit once every 60-90 minutes. In the laboratory, this variation in orbital lighting is simulated by mounting the orbital light source on a moving platform with computer controlled translation, pan, tilt and intensity controls. As the translating light source is on a straight track and not a curved track, the focus/intensity controls allows for the compensation of the different distances between the lamp and the object being inspected.

3. Power budgets being limited on spacecraft, on-orbit controlled illumination is of limited power and hence the option of using bright controlled lighting to overpower the solar illumination is precluded. Effectively, the light levels provided by the controlled illuminators at the surface of interest will be at or below the level of the ambient solar illumination. The impact of this is especially great on any scheme designed to compensate for the variability in the ambient light as will be discussed in Section xx. In the laboratory, two controlled lights are mounted on the end-point of the manipulator arm to provide the close-up illumination and to light enclosed or shadowed regions. A strobe illuminator with the same total light energy from xxx corp, is also available at the end of the manipulator arm. Lighting angle can be adjusted for diffuse or specular illumination with typical configurations at a compromise illumination angle.
4. Camera platforms on a telerobotic arm for space inspection need to be compact so as to provide a small convenient package for closeup inspection of surfaces and access to hard to reach spots. In addition to being of small size the other requirement for the cameras is to have an adequate dynamic range to enable the inspection. The cameras used in our laboratory for the robot arm mounted in inspection are Panasonic GP II, SJ 02 model CCD image sensor with 682(H) x 492(V) pixels. The camera head has a mass of 16g and is very compact.
5. The inspection targets often incorporate specular materials and the image is usually contaminated by highlights and shadows.
6. Erosion of surfaces due to atomic oxygen and ultraviolet exposure can change the reflectivity of the surface thereby increasing the likelihood of false triggers.
7. The objects themselves have complex 3-dimensional shapes and do not present a flat target for easy imaging, thereby requiring the development of compensation methods to remove distortions.
8. A variety of object and flaw types must be accommodated.
9. Slight positioning errors in the robot arm carrying the imaging platform results in imprecise positioning of the cameras with respect to the target.
10. Repeatedly starting and stopping a robot arm to take images could result in unnecessary power consumption, excessive operational time due to the settling time of the arm, and increased disturbances induced onto the spacecraft structure. It therefore becomes desirable to performing the inspection from a continually moving sensor platform, with the attendant problems of motion blur and increased imprecision in platform positioning.

3.1 Image Differencing For Change Detection

The baseline system utilizes an image comparison method that checks for differences between an earlier *reference* image of the unflawed object with a later *inspection* image of the object to detect and localize possible flaw regions. Computer controlled illuminators are used to compensate for variability in ambient lighting which would otherwise give rise to different shading, highlighting and shadowing patterns in the *reference* and *inspection* images. The technique takes two images each for the *reference* and *inspection* images, the first illuminated only with the ambient light and the second illuminated with the ambient light as well as the controlled illuminators. The information in the first image is subtracted from that in the second giving rise to a compensated image that appears as if it were taken with the controlled lights alone in the presence of no ambient illumination, with however a halving of the S/N ratio.

In order for the subtraction results to be valid, the sensor response to the illumination must be linear. The CCD response is calibrated and a compensation table is used to convert the normal square-root shaped response to a linear one. If strobe illumination is utilized, then the 2 : 1 interleaved fields of the camera allows one to perform intra-frame subtraction to obtain an ambient compensated (but with lower vertical resolution) image. This is preferable when the camera platform is in motion since it avoids many of the misregistration problems between the ambient lit and ambient plus controlled lit images.

The comparison of these compensated images is much easier than that of the uncompensated images and can be implemented in the form of a simple subtraction. However, slight differences in camera platform locations used during the taking of the *reference* and *inspection* images result in misregistration of the images and complicates the image comparison process

i.e. simple subtraction will give rise to a number of "false edges" in the images. A variety of ways have been investigated for correcting this misregistration. The first involves identify features in the *reference* image, estimating their displacement in the *inspection* image, and computing a least square image warping transform to deform the *inspection* image prior to performing the subtraction. The second technique utilize the fourier transform of the row/column sum of the image pixel data to estimate x-y misregistration and uses a shift operation to displace the *inspection* image. Finally, morphological erosion operations are used to remove "false edges" introduced due to any residual misregistration. This approach is however only useful if the flaw being sought does not get eliminated by the morphological operations.

The overall results of the differencing operations are illustrated in a simple example shown in Figure 1 where a missing screw on a radiator assembly is located by comparing a *reference* and *inspection* images. The differencing methods runs on a real-time Datcube image processing hardware system.

4 Scale Space

In the design of tele robotic vision systems two principal factors demand careful consideration: First there is always a human-in-the-loop of operations. Second, the human operated local site and the remote inspection site, where the robot operates, are physically separated by large distances. The first factor calls for a robot vision system design that incorporates the preprocessing of images, for display to the remote human operator, in such a manner as to highlight image features at "relevant Scales". This requirement stems from the fact that for a given inspection task only a limited range of image scales are relevant [7] to human observers. For example, if the task is to inspect a surface for "defects" about one centimeter in diameter, presenting an image of the scene with a field-of-view (FoV) that is either too large (of the order of meters) or too small (of the order of micrometers) will not provide any relevant information to the human operator. The second factor calls for the efficient representation of images for transmission over large distances.

With a view, to address both these factors and to overcome some of the image registration difficulties described in the previous sections, a scale-space [8] approach incorporating a pyramidal representation [9] of images has been adopted in our work. The princi-

ples of the scale-space and pyramidal approaches will be outlined next, followed by a detailed description of our approach, including examples of our results.

Scale-space is easily explained in two dimensions: One dimension in this space is a spatial dimension, such as the spatial distance between two edge-points. The second (orthogonal) dimension is scale - which can take one of two scalar forms - *inner-scale* or *outer-scale*. Visual information is constrained by the choice of these two scalar quantities. The inner-scale is determined by the resolution limit of the sensor (Human-eye, camera) and the outer-scale is determined by the FoV of the sensor. Human eyes, for example have about a 1 minute of arc visual angle resolution and a 120 degree visual angle horizontal FoV. Changing either one of these scales by using a lens can drastically alter the visual information recorded and hence can alter the outcome of any detection and classification process. As the scale parameter is increased the spatial distance between edges decreases (since the edges blur) until finally at a particular scale the edges blur into one another. The locus of the two edge points formed by varying the scale parameter is known (in recent machine vision research) to create a useful and robust feature signature.

The "pyramidal" approach [9] consists of systematically generating decreasing resolution representations of an original image. Pyramids can be generated by either convolving Gaussian kernels, with increasing variances and support, with the original image or by convolving a fixed Gaussian kernel with the original image first, and then with the resulting convolved images. The latter approach is adopted in our work, with a fixed separable 5×5 kernel being used. The Gaussian kernel adopted has binomial coefficients along a separable direction given by $\frac{1}{16} [1, 4, 6, 4, 1]^T$. At the base of such Gaussian pyramids is the original image (denoted by G_0) and at its apex is a single-pixel image (G_n) which represents the "mean" brightness associated with the entire original image. Every intermediate level in a Gaussian pyramid going from the base upwards to the apex, contains mean-values of larger and larger sub-regions of the original image. Typically each level in a Gaussian pyramid is decimated (by discarding every other row and column of the convolved image) and hence reduced 4 times in pixel-count before being stored. The reason for this decimation is that each convolution introduces a reduction in high spatial frequency content of the image and thus allows image sub-sampling (or decimation) without much loss of information.

While Gaussian pyramids give noise reduced esti-

mates of the mean value associated with image sub-regions, information pertaining to another important image statistic - the pixel intensity variance across an image sub-region - is not directly given at any level of the pyramid. Pixel intensity variance is important because it is directly related to the presence of edges, and edges form the basis of spatial feature classification. In theory, one should directly use an edge detector (such as a Laplacian or a Canny edge detector) at each level of the Gaussian pyramid to detect edges, instead of having to estimate edges from intensity variances. But edge detectors are usually unstable in the presence of noise (Laplacian) or are optimal only with specific noise statistics (Canny is optimal in the presence of Gaussian noise). In addition edge detection is an added computational overhead.

There is a close computational equivalent of the Laplacian edge detector, which one can use in practice to extract edges from Gaussian pyramids. This equivalent to the Laplacian operator is the difference-of-Gaussian (DoG) operator. DoG operations are effortlessly carried out using Gaussian pyramids by subtracting successive levels of the Gaussian pyramid (prior to decimation). Such pyramids are referred to as "Laplacian" pyramids and their i th level L_i is obtained using the relationship: $L_i \equiv \{G_{i-1} - G_i\}$, where the tilde is used to indicate an undecimated image.

5.1 Procedure and Results

To perform the automated inspection task involving image differencing for defect detection and scale-space pyramidal analysis for defect feature extraction, the following multiphase procedure is suggested: First create a *reference* image database that can be queried using the positional information of the robot cameras, the scene lighting conditions and the date of image-capture. These *reference* images are obtained using both the ambient and controlled illuminators. Next record images at the desired inspection sites and perform image-differencing to detect changes in the image-content. Finally perform a scale-space analysis of the images at the desired regions of-interest, and extract features to be used in defect classification. The procedure at inspection time is thus summarized as follows: (1) Capture *inspection* images using ambient and controlled illumination. (2) Obtain the "difference image" as follows: (2a) First create a compensated *reference* image ($\hat{R} = R_c - R_a$) and a compensated *inspection* image ($\hat{I} = I_c - I_a$), where "R" denotes the *reference*

images and "I" denotes *inspection* images. The subscripts "a" and "c." denote lighting conditions *ambient* and *controlled* lighting, respectively. The "hat" on R and I denotes compensation. (2b) Next subtract \hat{R} from \hat{I} to obtain the difference image D of the desired inspection site. (3) Form a Gaussian pyramid [9] to represent a given image at a range of resolutions ("iriller-scale"). (4) Given the physical size of the defects being searched for, select the most relevant levels (scales) of the Gaussian pyramid. (5) Perform image differencing at the relevant scales. (6) Select candidate regions of-interest based on highlights of the "difference image". (7) Eliminate those regions which are highlighted for extraneous reasons such as specularities in the original image or image misregistration. (8) For each "defect-region" identified, perform edge-detection and feature extraction. (9) Finally, for each of the defects detected and identified, present the human operator with a probabilistic estimate, based information from a historical database, of the potential danger posed by the defect.

The application of the above procedure is illustrated in the composite Figure 2 which utilizes a combination of the differencing and scale-space approach to find micrometeoroid damage to a r/wc-kill, of a truss assembly mounted orbital replacement units (ORU). The compensated *inspection* image is obtained from I_a (2c) and I_c (2d), and the compensated *reference* image is obtained from image R_a (2a) and R_c (2b). The difference image D (Fig. 2f) contains the new information in the compensated *inspection* image with respect to the compensated *reference* image. Unlike the images in 1 we have deliberately used an incorrectly linearized CCD sensor, and have not corrected for misregistration in order to demonstrate the robustness of the scale space flaw recognition approach. The new information in image D thus comes from not only damage on the surface but also from image misregistrations and poorly compensated specular highlights.

The "spurious" highlights have been filtered out. One method that was applied to deal with this problem was to examine the pixel intensity profiles of the various regions of the difference image. Figure 3a shows profiles of a specular point (Fig. 3b), a surface defect (Fig. 3c) and a region of misregistration (Fig. 3d). Notice that the profile of the defect has only positive differences, whereas the profiles of the specular point and the misregistered region have both positive and negative differences. Figure 2f shows a small region of 2c in greater detail. This detail shows the nature of the surface defects under scrutiny - a spotted collection of

bright spots together with a relatively large fractal like region in the lower right of the image. This image corresponds to a physical outer-scale (FoV) of about 2cm x 2cm. If the inspection task is for 1cm sized features, then it is important to emphasize those spatial frequencies in the original difference image that emphasize objects of 1cm size. To accomplish this end, the difference image D (Fig. 2c) is represented in a Gaussian pyramid, containing successively low-passed version of I . This is shown in Figures 2g-l. The image with the inner-scale most distinctly displaying 1cm sized features is shown in Figure 2h. On either sides of this image are a higher frequency content version (Fig. 2g) and a lower frequency version (Fig. 2i). While the physical dimension of the image D is of the order of 250K pixels, the dimensions of the image with the relevant scale (Fig. 2h) is only of the order of 10K. Clearly showing about a 25 fold decrease in the amount of processing required.

Figure 4 shows the result of performing a Canny edge detection on images at the three desirable scales corresponding to images in Figures 2g-i. For each of the edges detected and shown in the form of rectangular boxes in the zoomed image seen in the second column, a set of features such as compactness, elongation, centroid location, ratios of perimeter-to-bounding box size have been extracted. These feature will form inputs to future pattern classification schemes. The histograms shown on the right columns of the Figure 4 show the number of pixels required to represent the displayed boxed images. The top histogram shows that in picking the defects about 4000 pixels are processed. The center histogram shows that about 1400 pixels are processed. The bottom histogram shows that if the task was to detect 1 cm sized blob like features which take the form of "hook" like features, then just about 200 pixels are required. This demonstrates the efficiency of scale-space processing.

6 Future Work

Flaw classification algorithms for specific flaw types are being investigated as well as the implementation of the scale-space flaw classifier on the real-time system. A more sophisticated statistical approach is being investigated to compare "before" and "after" images based on certain ideas from invariant image perception. A & D smoothing algorithm is being developed will be used to compensate for variations in object shape and extract a surface texture/feature model which may then

be classified. Multispectral data in the form of color and IR is also being incorporated.

7 Summary and conclusions

A comprehensive automated inspection system, involving telerobotic operations on remote space platforms has been described. Special design considerations, taking into account the "human-in-the-loop" nature of telerobotic operations, have been used in the development of the algorithms for surface inspection. Examples of applying the algorithms to the task of automatically inspecting model orbital-replacement units, have been provided. Guidelines for future work has D'Elia suggested. The success of automated inspection system design for telerobotic operations depends on a quantitative understanding of the joint performance of robotic sub systems and human operators. Our results provide some initial insight to such performance studies.

Acknowledgments

The research described in this document was performed at the Jet Propulsion Laboratory, California Institute of Technology, under contract with the National Aeronautics and Space Administration. The first author would also like to acknowledge support from the Beckman Institute of the California Institute of Technology. We would also like to acknowledge the technical support of G. Rodriguez, D. Gemery and M. van Nieuwstadt.

References

- [1] See, **'1'**, et. al, "Meteoroid and Debris Impact Features Document on the Long Duration Exposure Facility: A Preliminary Report", Space and Life Science Branch Publication No. 84, NASA No. 24608, August 1990.
- [2] Fisher, F. and C.R. Price, "Space Station Freedom External Maintenance Task Team - Final Report", Vol. 1, NASA, JSC, Houston, TX, July 1990.
- [3] S. Hayati, et. al, "Remote Surface Inspection System", in *Proceedings SOAR Conf.*, Houston, Texas, 1992.
- [4] H. Seraji, "Configuration Control of Redundant Manipulators: Theory and Implementation," *IEEE*

Trans. on Robotics and Automation, Vol. 5, No. 5, 1989, pp. 472-490, 1989.

- [5] R. T. Chin and C. A. Harlow, "Automated Visual Inspection: A Survey", *IEEE Trans. Pattern Analysis and Machine Intelligence*, vol. PAMI-4, No. 6, Nov. 1982.
- [6] K. Isoda, "Advanced Robot ic Inspection Applications," in *International Encyclopaedia of Robotics*, Ed. R. Dorf, John Wiley and Sons, Vol 2, pp. 668-679.
- [7] Koenderink, J. J., "The Structure of Images," *Biol. Cybern.*, Vol. 50, pp. 363-370, 1984.
- [8] Witkin, A. P., "Scale-space Filtering," *Proceedings IJCAI*, pp. 1019-1022, Karlsruhe, Germany, 1983.
- [9] Burt, P. J., "Multiresolution techniques for image representation, analysis, and 'smart' transmission," *SPIE Conf. 1199: Visual Communications and Image Processing IV*, Philadelphia, Nov. 1989.

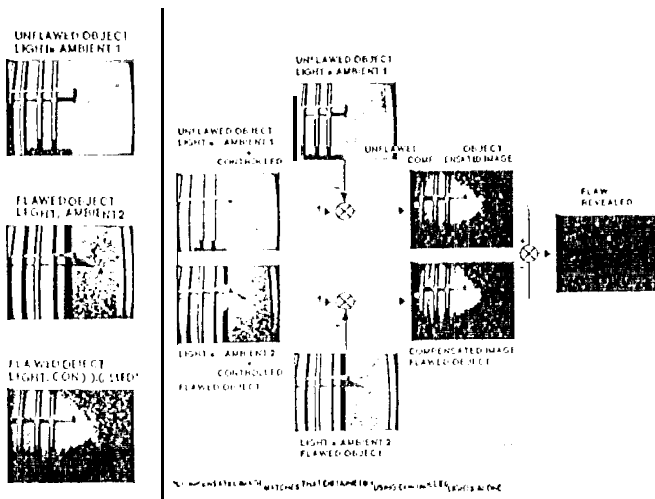


Figure 1: Flaw Detection by Image Differencing: The final image subtraction after correction for registration errors reveals the missing screw

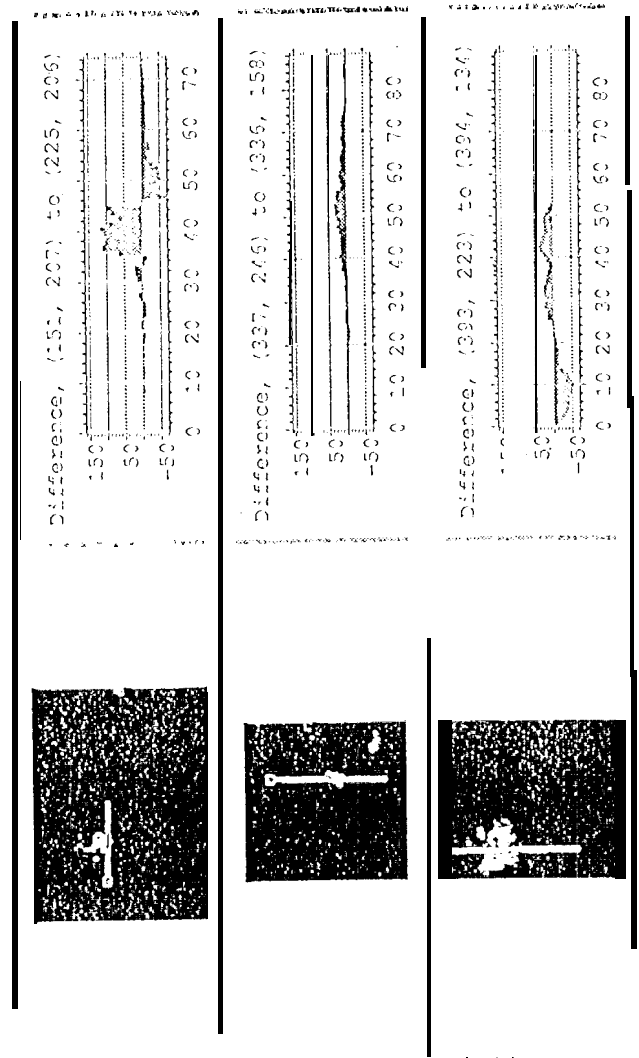


Figure 3: Flaw Profiles: The top row shows a specular highlight, the second row shows a relevant defect (with positive histogram) and the bottom row shows a registration induced highlight.